International Journal of Mass Spectrometry 282 (2009) 112–122

Contents lists available at ScienceDirect

International Journal of Mass Spectrometry

journal homepage: www.elsevier.com/locate/ijms

Composite field approximations for ion traps with apertures on electrodes

Madhurima Chattopadhyay[a], Neeraj Kumar Verma[b], Atanu K. Mohanty[a,b,*]

[a] Department of Instrumentation, Indian Institute of Science, Bangalore 560012, India
[b] Supercomputer Education and Research Centre, Indian Institute of Science, Bangalore, Karnataka 560012, India

ARTICLE INFO

Article history:
Received 15 December 2008
Received in revised form 13 February 2009
Accepted 13 February 2009
Available online 10 March 2009

Keywords:
Axially symmetric (3D) trap
Two dimensional (2D) trap
Boundary element method (BEM)
Electric field in the vicinity of aperture
Multipole

ABSTRACT

This paper presents two approximate analytical expressions for nonlinear electric fields in the principal direction in axially symmetric (3D) and two dimensional (2D) ion trap mass analysers with apertures (holes in case of 3D traps and slits in case of 2D traps) on the electrodes. Considered together (3D and 2D), we present composite approximations for the principal unidirectional nonlinear electric fields in these ion traps. The composite electric field E has the form

$$E = E_{\text{noaperture}} + E_{\text{aperture}},$$

where $E_{\text{noaperture}}$ is the field within an imagined trap which is identical to the practical trap except that the apertures are missing and E_{aperture} is the field contribution due to apertures on the two trap electrodes. The field along the principal axis of the trap can in this way be well approximated for any aperture that is not too large.

To derive E_{aperture}, classical results of electrostatics have been extended to electrodes with finite thickness and different aperture shapes.

$E_{\text{noaperture}}$ is a modified truncated multipole expansion for the imagined trap with no aperture. The first several terms in the multipole expansion are in principle exact (though numerically determined using the BEM), while the last term is chosen to match the field at the electrode. This expansion, once computed, works with any aperture in the practical trap.

The composite field approximation for axially symmetric (3D) traps is checked for three geometries: the Paul trap, the cylindrical ion trap (CIT) and an arbitrary other trap. The approximation for 2D traps is verified using two geometries: the linear ion trap (LIT) and the rectilinear ion trap (RIT). In each case, for two aperture sizes (10% and 50% of the trap dimension), highly satisfactory fits are obtained. These composite approximations may be used in more detailed nonlinear ion dynamics studies than have been hitherto attempted.

1. Introduction

This paper develops composite analytical approximations to describe electrostatic fields within axially symmetric (3D) and two dimensional (2D) ion trap mass analysers.[1] The composite approximation developed provides a description of the field right from the center of the trap up to and just beyond the apertures on the electrodes, along the principal axis of the mass analyser. This may be contrasted with the hitherto available multipole expansions, which are local expansions for the field near the trap center, and break down near the trap apertures. We see the greatest relevance of this work, as we will discuss in greater detail at the end of the paper, in miniaturized traps, where aperture sizes may not scale down equally as overall trap dimension, necessitating a better understanding of their effects on fields in such traps.

This work can be motivated as follows. In the literature, the dynamics of ions in rf traps has been studied by many investigators [5,9,18] who considered, essentially, an equation of motion of the form:

$$\frac{d^2u}{d\xi^2} + (a - 2q\cos 2\xi)f(u) = 0. \quad (1)$$

When $f(u) = u$, we have the Mathieu equation, relevant to the ideal Paul trap. For small trap imperfections or motions close to the trap center, $f(u)$ is a weakly nonlinear function of u. For traps with non-hyperboloid geometry, and when we are interested in

* Corresponding author at: Supercomputer Education and Research Centre, Indian Institute of Science, Bangalore, Karnataka 560012, India. Tel.: +91 80 2293 2979; fax: +91 80 2360 0135.
E-mail addresses: madhuri@isu.iisc.ernet.in (M. Chattopadhyay), neeraj.iisc@gmail.com (N.K. Verma), amohanty@serc.iisc.ernet.in (A.K. Mohanty).

[1] Throughout this paper the descriptor 3D refers to traps with axial symmetry, and 2D to traps with planar symmetry. It should be noted, however, that the fields in both these traps are three-dimensinal. In our analysis we use the symmetry to simplify the analysis and carry out a two-dimensional analysis of these traps.

1387-3806/$ – see front matter © 2009 Elsevier B.V. All rights reserved.
doi:10.1016/j.ijms.2009.02.022

dynamics including motions approaching the electrodes, we must account for strongly nonlinear $f(u)$. This paper presents expressions for the electric field that in turn determines what $f(u)$ is. The dynamics arising therefrom are left for future work.

In our composite approximation for the field alluded to above, some constant coefficients need to be evaluated numerically for a trap with no aperture on the electrodes. After this, the field due to apertures, from classical results [20,6], is added on analytically to obtain a composite approximation. This approximation is the first such description in the mass spectrometry literature. It provides an explicit formula for the contribution of the apertures in the electrodes to the field within the trap, and is usefully accurate over the entire extent of the trap along its principal direction.

The mass analyser of an ideal ion trap mass spectrometer consists of hyperbolic shaped electrodes. In the 3D Paul trap [13], the mass analyser has three hyperbolic shaped electrodes with two (electrically shorted) end cap electrodes and one ring electrode. The 2D LIT [3] consists of four hyperbolic shaped longitudinal electrodes with the two opposite pairs of electrodes being electrically shorted. In the ideal traps, the electrodes are not truncated and there are no apertures in the electrodes (in the 3D trap, the apertures are the holes on the two endcap electrodes and in the 2D trap they are the slits on the two opposite electrodes). When an rf-only or rf/dc potential is applied across the electrodes, a linear trapping field is created within the trap. Fragment ions of an analyte gas are trapped at the center of the trap in the 3D traps and along the longitudinal axis in the 2D traps. The motion of ions as well as the stability of the ion motion is described by the Mathieu equation [11,10].

The practical trap differs in its geometry in two significant ways from its ideal counterpart. First, although the electrodes of the practical trap continue to have hyperbolic shapes, holes or apertures are introduced in the electrodes for entry of electrons and exit of destabilized fragment ions. In addition, the electrodes are truncated to finite size to reduce their dimensions to manageable proportions. While these are intentional alterations carried out on the electrodes, a few inadvertent modifications such as misalignment in the positioning of electrodes, fabrication errors of the hyperbolic profile and uneven spacing between the electrodes further alter the geometry of the practical trap. A second way in which some practical traps differ from the ideal 3D and the 2D structures are in the shape of the electrodes. The electrodes of these newer traps no longer have hyperbolic profiles but instead have easily machinable simple profiles. Examples of such traps are the 3D cylindrical ion trap (CIT) [8,21] and the 2D rectilinear ion trap (RIT) proposed by Ouyang et al. [12]. The 3D CIT consists of two flat endcap electrodes and a cylindrical ring electrode while the 2D RIT consists of four flat plate electrodes. These electrodes too are truncated to finite size and they have apertures in them.

An important consequence of this alteration in geometry is that the field within the trap is no longer linear and the linear Mathieu equation can be used to describe the motion and stability only close to the center of the trap where the field can be assumed to be linear. To understand ion dynamics in these nonlinear devices, researchers have resorted to numerical simulations (e.g., Franzen et al. [5]) or, when analytical approach was required, used the multipole description of the field using Legendre polynomials [2]. Examples of the latter studies include those of Makarov [9], Sudakov [18], Abraham et al. [1], Rajanbabu et al. [15,16]. An important aspect of these latter studies was that they focussed on the destabilization dynamics of the ions near the trap center and were not concerned with large amplitude oscillations in the trap. Relatively few multipole weights sufficed to describe the field near the trap center. When ion oscillation amplitudes grew and ions approached the trap boundary, where larger multipole weights became important, ions were considered already unstable and it was assumed that their motion was not affected by the fields close to the apertures on the electrodes through which they were ejected.

Although there have been some limited discussions [14,19] on the contribution of holes on the electrodes to the field in the 3D trap, an analytical description of the field within the entire trap has not been available even for the standard practical trap. Plass et al. [14] have, for instance, suggested the use of higher order multipoles to characterize the field close to the electrodes, but if solely higher order multipoles were to be used, then it would require many terms to accurately describe the field near the discontinuities on the electrodes caused by the apertures. In this paper, we present a viable alternative.

Our motivation in this paper is to develop an accurate analytical expression for the field in practical axially symmetric (3D) and 2D traps which have apertures on their electrodes. The expression we present will focus on the field only along the principal axis of the trap, along which ion destabilization takes place.

After a brief description of the numerical method used by us in the next section, we carry out a numerical study of the field in the CIT in Section 3 to show that varying hole size does indeed alter the field within the trap. We next present an overview of the approach adopted by us. This is followed by, in Sections 5 and 6, the development of the expression for the field in the 3D and the 2D geometries, respectively. In Section 7 approximate analytical expression is tested on a few arbitrary geometries. Finally, in Section 8, we present a few concluding remarks.

2. Numerical methods

To compute the field numerically for any ion trap having a symmetric geometry, we have developed a library which is based on the boundary element method (BEM). By using this library, we can easily define any trap geometry and can also specify the potential applied to the electrodes.

The BEM based field computation has two steps. First, charge distribution on electrodes is determined from the known applied potential on the electrodes and second, the potential (and the field) at any point in space is computed from the charge distribution on the electrodes by the principle of superposition.

In order to compute charge distribution on the electrodes, the electrode surfaces are divided into small regions or elements. Let the total number of such elements be N and let v_i be the potential applied to ith element, $G_{i,j} = g(i,j)$ be the potential at ith element due to unit charge at jth element. The unknown charge q_j is computed using the principle of superposition from the expression

$$\sum_{j=1}^{N} g(i,j)q_j = v_i, \quad i = 1, \ldots, N, \tag{2}$$

where $g(i,j)$ is called the Green's function. Unknown charges q_j can be found by solving linear system of simultaneous equation (Eq. (2)) provided $g(i,j)$ is known. The Green's function for 3D geometries has been derived in Tallapragada et al. [19] and the 2D Green's function has been discussed in detail in Krishnaveni et al. [7]. The computation of field and multipole coefficients from the numerically obtained charge distribution has also been discussed in those two papers.

3. Numerical study of the field in the CIT with different hole sizes

To demonstrate that the apertures do alter the field within the trap, we numerically investigate the CIT proposed by Wu et al. [21] as an example. The cross-sectional view of the CIT with geometry parameters are presented in Fig. 1 (a) and the dimensions (in mm)

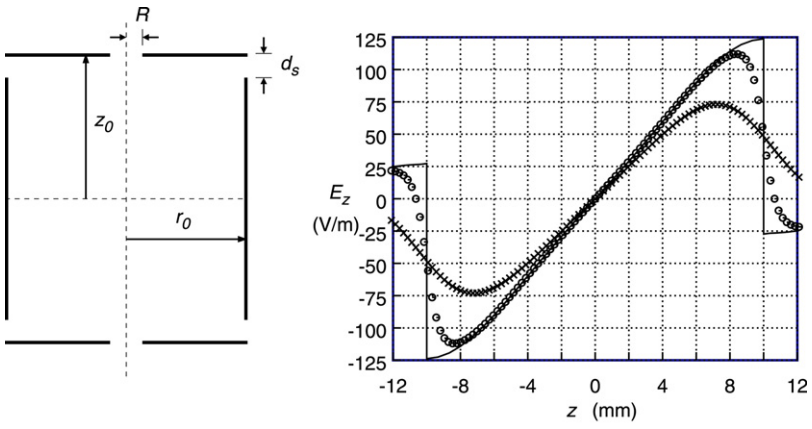

r_0	z_0	d_s	R
10	10	1.6	1.0(circle), 5.0(cross)

Fig. 1. (a) Cross-section view of the CIT with its dimensions given in the table below. (b) Numerically obtained field for trap having no hole and 1 mm (circle) hole radius and 5 mm (crosses) hole radius. All dimensions of geometry parameters given in the table are in mm.

used in our computations have been given in the table below the schematic. We have assumed that the electrodes have no thickness. In our simulations, the endcaps have been kept at ground potential and the ring electrode at unit positive potential.

Fig. 1(b) is a plot of the numerically obtained field (in V/m) versus distance from the centre of the trap (in mm). The plot of the field has been made to a distance just beyond the endcap electrode. The discontinuous curve is the field variation in a trap which has no holes on the endcap electrodes. The continuous curves superimposed by circles and crosses correspond to a trap which has hole sizes corresponding to 1 mm (10%) and 5 mm (50%) of the trap radius, respectively.

It is apparent that introducing the hole has resulted in the field across the endcap electrode becoming smooth (that is, the hole has the effect of eliminating the discontinuity). As the hole radius increases, the field in the vicinity of the hole weakens, although close to the center of the trap there is no significant variation in the field with hole size. These simulations demonstrate that the dimension of the hole radius in the endcap electrodes does indeed alter the field within the trap, especially in the vicinity of the endcap electrodes.

4. Our approach

We assume that the field within a practical trap can be obtained by superposing the field in a trap with no aperture with the field contribution of the apertures. Consequently, we write

$$E = E_{\text{noaperture}} + E_{\text{aperture}}, \tag{3}$$

where E is the field within the trap that we are seeking to find an analytical expression for, $E_{\text{noaperture}}$ is an analytical expression for the field within the trap with no apertures and E_{aperture} is an analytical expression corresponding to the contribution of the aperture to the field in the vicinity of the aperture.

In this paper we will first develop an expression for E_{aperture}, the contribution of aperture to the field. Starting with an aperture in an infinitely thin, conducting plane, the field expression for which is available in literature, we extend it to apertures in electrodes with finite thickness. In this expression the dimension of the aperture is a free parameter in this expression.

Following this, we develop an analytical expression for $E_{\text{noaperture}}$. For this we use a truncated multipole expansion to represent the field within a trap which has no apertures on its electrodes. Relatively few terms suffice to describe the field in a large region of the trap and a deviation is observed only close to the trap electrodes. To bring about a match (with the numerically obtained field) near the electrodes we modify the truncated multipole expansion by adding an extra term to correct for the field deviation near the electrodes. All constants in the modified multipole expansion expression are evaluated numerically.

With these two expressions incorporated in Eq. (3), we can estimate the field within the trap for any reasonable hole size. In our present work we have shown the utility of this expression for an aperture size upto 50% of the size of the trap.

5. Fields in 3D traps

5.1. Contribution of the hole to the field

Having seen that the size of the hole on the endcap electrode does indeed alter the field within the trap, we will next turn to understand the contribution of the hole to the field within the 3D trap. To understand the effect of the hole in the endcaps we first consider the problem of a hole in an infinitely thin, conducting plane as discussed in the literature [6]. Although this derivation is for a thin plate, we will develop a theory capable of dealing with finite width thick endcaps which are used in practical ion traps. Even though the theory is exact for an infinite flat plate, our results will demonstrate that even for traps with curved endcaps, the theory predicts fields accurately.

The field distribution on either side of an infinitely thin, conducting plane having no hole and with a uniform field E_0 and E_1 (as seen in Fig. 2 (a)) on either side can be expressed as

$$E_{\text{nohole}}(z) = \begin{cases} E_1 & \text{if } z > 0, \\ E_0 & \text{if } z < 0. \end{cases} \tag{4}$$

In the above and in what follows, all fields are understood to be purely in the principal direction (here, z; and for the 2D case, y) due to symmetry, and so only the scalar component in the principal direction is dealt with.

To get an expression for the contribution of the hole to the field within the trap, we will need to subtract the field when there is no hole on the electrode from the field in the presence of a hole of radius r on the electrode. This difference in field will give us the contribution of the hole to the field.

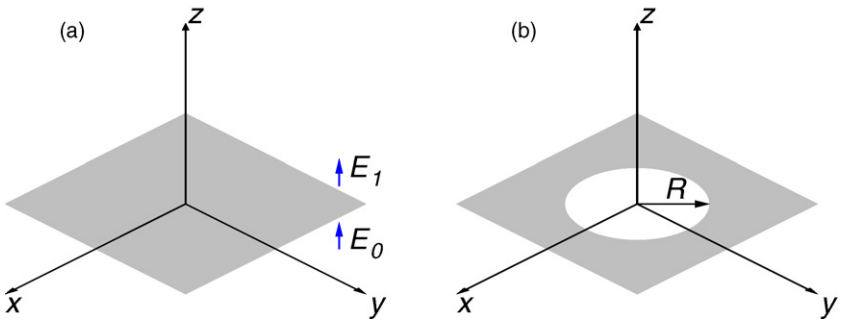

Fig. 2. (a) Schematic of an infinite thin metal plate with fields $E_0\hat{z}$ and $E_1\hat{z}$ on either side and (b) the same plate with a circular hole of radius R.

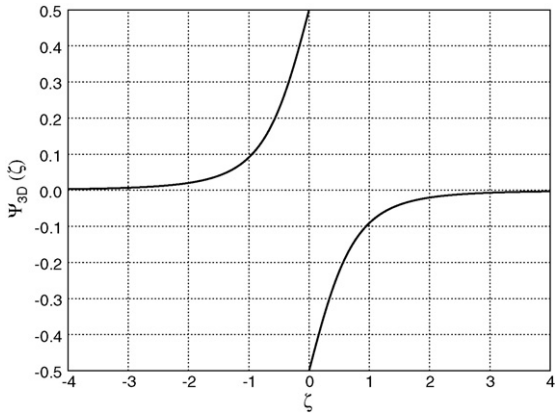

Fig. 3. Plot of the function $\Psi_{3D}(\zeta)$, which appears in expressions for the field contribution due to the hole.

To get an analytical expression for the contribution of the hole to the field we begin by considering the field along the axis of the infinitely thin, conducting plane, with constant fields E_0 and E_1 on either side. This problem has been widely discussed in classical literature and we adopt, in our present study, an expression provided in Jackson [6]. In the presence of hole of radius R (Fig. 2(b)), the expression for the field across an infinitely thin, conducting plane, $E_{\text{withhole}}(z)$, is given by

$$E_{\text{withhole}}(z)=\frac{(E_1+E_0)}{2}+\frac{(E_1-E_0)}{\pi}\left[\arctan(z/R)+\frac{z/R}{(z/R)^2+1}\right], \quad (5)$$

where z refers to the distance from the center of the hole.

The contribution of the hole can now be evaluated by subtracting Eq. (4) from Eq. (5). This yields

$$E_{\text{withhole}}(z)-E_{\text{nohole}}(z)=-\frac{(E_1-E_0)}{2}\text{sign}(z/R)+\frac{(E_1-E_0)}{\pi}\left[\arctan(z/R)+\frac{z/R}{(z/R)^2+1}\right], \quad (6)$$

which can be written as

$$E_{\text{withhole}}(z)-E_{\text{nohole}}(z)=\Delta E\left[-\frac{\text{sign}(z/R)}{2}+\frac{1}{\pi}\left(\arctan\left(z/R\right)+\frac{z/R}{(z/R)^2+1}\right)\right] \quad (7)$$

by substituting (E_1-E_0) by ΔE. Hence, the contribution of the hole, $E_{\text{hole}}(z)$, can be written as

$$E_{\text{hole}}(z)=E_{\text{withhole}}(z)-E_{\text{nohole}}(z)=\Delta E\Psi_{3D}(z/R), \quad (8)$$

where

$$\Psi_{3D}(\zeta)=-\frac{\text{sign}(\zeta)}{2}+\frac{1}{\pi}\left(\arctan(\zeta)+\frac{\zeta}{\zeta^2+1}\right). \quad (9)$$

A plot of Ψ_{3D} is given in Fig. 3.

In the case of the practical trap, as shown in Fig. 1(a), which has two electrodes and in which the origin of the co-ordinate system is conventionally chosen as the center of the trap, z/r may be replaced by $(z-z_0)/R$ for the upper endcap and by $(z+z_0)/R$ for the lower endcap. With this substitution we will have two expressions which

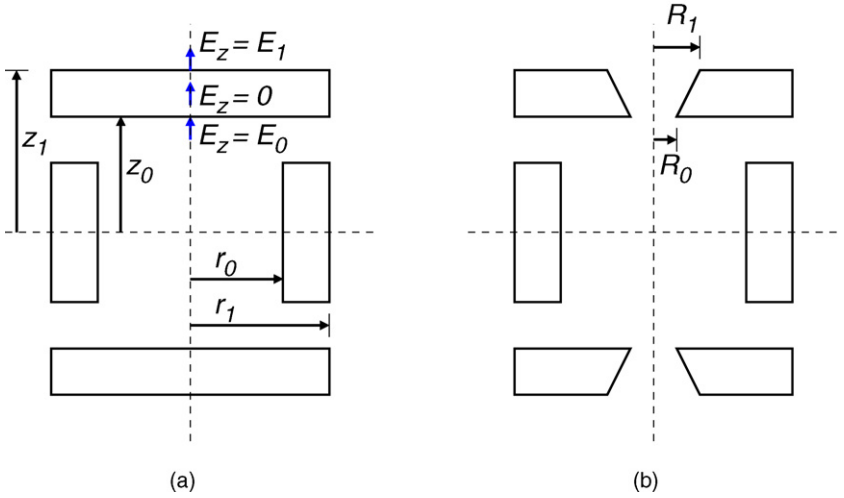

Fig. 4. (a) Schematic of a CIT with thick electrodes with no holes. (b) The same CIT in which the endcaps have holes.

describe the contribution of the holes on the two endcaps to the field within the trap.

To get the expression for the field within the trap we need to add the field contributions of the hole in the two endcap electrodes (Eq. (8)) to an as yet unevaluated term $E_{\text{nohole}}(z)$. $E_{\text{nohole}}(z)$ corresponds to the field within the trap when there are no holes in the endcap electrodes. Thus the expression for field within the trap, $E_{3D}(z)$, will have the form

$$E_{3D}(z) = E_{\text{nohole}}(z) + (\Delta E)_{z=z_0}\Psi_{3D}\left(\frac{z-z_0}{R}\right) + (\Delta E)_{z=-z_0}\Psi_{3D}\left(\frac{z+z_0}{R}\right). \quad (10)$$

In the above equation the first term corresponds to the field within the trap when there are no holes in the endcap electrodes and the second and third terms correspond to the field contribution of the holes in the top and bottom endcap electrodes, respectively.

Since there is top-bottom symmetry in our trap geometry, $(\Delta E)_{z=z_0} = (\Delta E)_{z=-z_0}$ and we will replace them by ΔE. The final expression then becomes

$$E_{3D}(z) = E_{\text{nohole}}(z) + \Delta E\left[\Psi_{3D}\left(\frac{z-z_0}{R}\right) + \Psi_{3D}\left(\frac{z+z_0}{R}\right)\right]. \quad (11)$$

Practical traps, of course, have endcap electrodes which have finite thickness. Our study has revealed that the effect of finite thickness of the electrode can easily be incorporated in the analytical expression by considering two infinitely thin electrodes to represent the thick electrode. Fig. 4 (a) is a schematic of a CIT with endcap electrodes having a thickness equal to $z_1 - z_0$ with no holes on the endcap electrodes. Fig. 4(b) is a schematic of the same CIT with holes in the endcap electrodes, one infinitely thin electrode having a hole of radius R_0, and the other having a hole of radius R_1, a situation corresponding to a bevelled hole being drilled on the endcap electrode. If the hole is straight, then $R_0 = R_1$.

An inspection of Fig. 4 indicates that for the upper endcap, the ΔE corresponding to the inner infinitely thin plate is $0 - E_0 = -E_0$, whereas for the top plate it is $E_1 - 0 = E_1$. The situation is also true for the lower endcap electrode. When these are introduced in the field equation we obtain the expression for E_{3D} as

$$E_{3D}(z) = E_{\text{nohole}}(z) + (-E_0)\left[\Psi_{3D}\left(\frac{z-z_0}{R_0}\right) + \Psi_{3D}\left(\frac{z+z_0}{R_0}\right)\right] + E_1\left[\Psi_{3D}\left(\frac{z-z_1}{R_1}\right) + \Psi_{3D}\left(\frac{z+z_1}{R_1}\right)\right]. \quad (12)$$

It is worth noting that when $z_0 = z_1$, and $R_0 = R_1$, Eq. (12) reduces to Eq. (10), which describes the field for endcaps with no thickness. Our next effort will be to obtain an analytical expression for $E_{\text{nohole}}(z)$.

5.2. $E_{nohole}(z)$

To obtain the analytical expression for $E_{\text{nohole}}(z)$, we begin by evaluating the field within the CIT (Fig. 1(a)). We will first use a numerically derived $E_{\text{nohole}}(z)$ to see if our Eq. (11) can be used to approximate the field within the trap.

To the numerically calculated field for the CIT presented in Fig. 1(a) in which $r = 0$ (that is the endcaps have no holes), we add the second term of Eq. (11)(the contribution of the holes in the two endcap electrodes) for a hole radius equal to 10% of the ring electrode radius.

Fig. 5 presents a comparison of the field obtained using Eq. (11)(circles) with that obtained entirely numerically (continuous line). The agreement between the two fields is seen to be excellent. This provides us a clue that if an analytical expression for $E_{\text{nohole}}(z)$ can be derived, we can use Eq. (11) for describing the field within the trap.

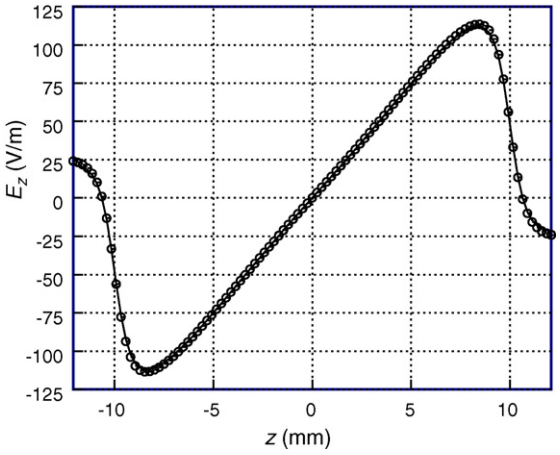

Fig. 5. Comparison of the fields within the CIT. Circles represent field obtained using Eq. (11); smooth curve represents field obtained numerically.

Among the different approaches that could potentially be used for providing an analytical expression to fit the numerical data for $E_{\text{nohole}}(z)$, we have chosen the use of the multipole expansion since this is a familiar technique in the mass spectrometry literature to represent the field in ion traps.

The potential at a point, $u(\rho, \theta, \phi)$, in spherical coordinates in an axially symmetric trap can be expressed as

$$u(\rho, \theta, \phi) = \Phi\sum_{n=0}^{\infty} A_n\left(\frac{\rho}{L}\right)^n P_n(\cos\theta). \quad (13)$$

Here Φ is the applied potential, A_n are the weights of the multipoles, P_n represents Legendre polynomial of n th degree, and L is the normalizing length. Potential at a point on z-axis can be found by putting $\theta = 0$ and $\rho = z$ in Eq. (13) to get

$$u(z) = \Phi\sum_{n=0}^{\infty} A_n\left(\frac{z}{L}\right)^n. \quad (14)$$

From the potential expression of Eq. (14) the electrical field along the z-axis can be expressed as

$$E_z(0,0,z) = -\frac{\partial u}{\partial z}(0,0,z) = -\Phi\sum_{n=0}^{\infty} nA_n\left(\frac{z^{n-1}}{L^n}\right) = \sum_{n=0}^{\infty}\alpha_n z^{n-1}, \quad (15)$$

where

$$\alpha_n = -\Phi\frac{nA_n}{L^n}. \quad (16)$$

Due to top bottom symmetry in geometries α_n for odd n is zero. Therefore,

$$E_z(0,0,z) = \sum_{k=1}^{\infty}\alpha_{2k} z^{2k-1}. \quad (17)$$

Using a truncated form of Eq. (17) upto M terms, we have

$$E_{z,\text{truncated}}(0,0,z;M) = \sum_{k=1}^{M}\alpha_{2k} z^{2k-1}. \quad (18)$$

Since our motivation is to get an analytical expression for $E_{\text{nohole}}(z)$ in Eq. (11), we will investigate how well the truncated multipole expansion (Eq. (18)) matches with the numerically obtained field for the CIT, shown in Fig. 1(a), but with no holes on the

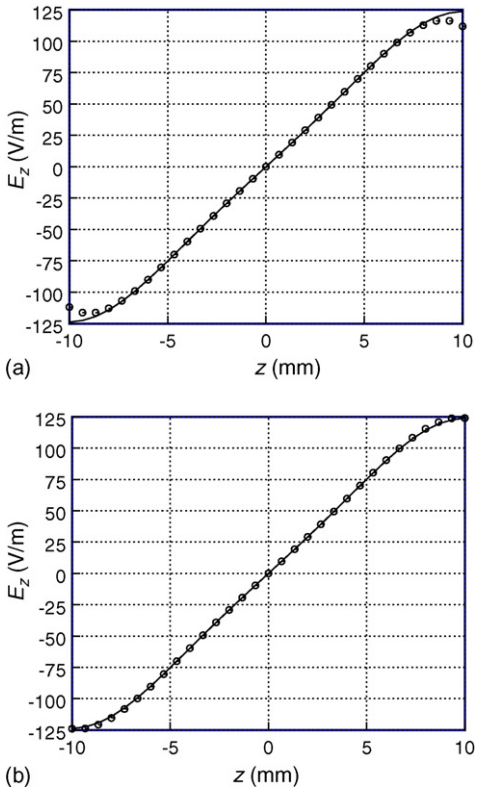

Fig. 6. Field along z-axis in CIT (no aperture). Continuous line represents numerically obtained field and circles represents the field obtained by (a) truncated multipole expansion and (b) with near electrode correction (no aperture).

endcap electrodes. To do this we have chosen relatively few terms in the expansion, up to $M = 3$.

Using the values of multipole weights (obtained numerically for the CIT with no holes on the endcap electrodes) in Eq. (18), we obtain a plot for the field which is shown in Fig. 6 (a), marked with circles. Also superimposed in this curve is the numerically obtained field for the CIT with no holes on the endcap electrodes. It can be seen that the two curves agree very well near the center of the trap but there is significant deviation close to the endcaps.

To improve the match between the two curves near the endcap electrodes, we propose a modified truncated multipole expansion by adding one additional higher order term, $\alpha'_{2(M+1)}z^{2M+1}$, to the expansion for representing the field by the Eq. (21). We require

$$E_{z,\text{modified}}(0,0,z) = \sum_{k=1}^{M}\alpha_{2k}z^{2k-1} + \alpha'_{2(M+1)}z^{2M+1} \tag{19}$$

to satisfy $E_{z,\text{modified}}(0,0,z) = E_0$, E_0 being the numerically estimated field at $z = z_0$. It should be noted that $\alpha'_{2(M+1)}$ is *not* the coefficient related to multipole weight $A_{2(M+1)}$, but is instead a constant introduced to match the numerical field at the electrode. Thus, the new coefficient $\alpha'_{2(M+1)}$ is obtained as

$$\alpha'_{2(M+1)} = \frac{\left(E_0 - \sum_{k=1}^{M}\alpha_{2k}z_0^{2k-1}\right)}{z_0^{2M+1}}. \tag{20}$$

The value of E_0, α_{2k} and $\alpha'_{2(M+1)}$ obtained for the CIT under study (which has no hole in the endcap electrodes) are reported in Table 1.

With the value of $\alpha'_{2(M+1)}$ reported in Table 1 inserted in Eq. (19), we plot the field within the trap in Fig. 6(b) with circles. The smooth curve corresponds to the numerically obtained field and

Table 1
Numerically obtained values of E_0, α_2, α_4, α_6 and α'_8.

E_0	α_2	α_4	α_6	α'_8
123.97	14.404	4.4267×10^{-2}	-7.6434×10^{-4}	1.2094×10^{-6}

it can be seen that Eq. (19) provides a very good description of the field between the two endcap electrodes in the CIT with no holes on the endcap electrodes. Consequently $E_{\text{nohole}}(z)$ can be represented by the expression

$$E_{\text{nohole}}(z) = \sum_{k=1}^{M}\alpha_{2k}z^{2k-1} + \alpha'_{2(M+1)}z^{2M+1}. \tag{21}$$

5.3. Electric field in the axially symmetric (3D) trap

The final composite analytical expression for the field in a 3D trap with electrodes of finite thickness has the form

$$\begin{aligned} E_{3D}(z) = & \sum_{k=1}^{M}\alpha_{2k}z^{2k-1} + \alpha'_{2(M+1)}z^{2M+1} \\ & +(-E_0)\left[\Psi_{3D}\left(\frac{z-z_0}{R_0}\right) + \Psi_{3D}\left(\frac{z+z_0}{R_0}\right)\right] \cdot \\ & +E_1\left[\Psi_{3D}\left(\frac{z-z_1}{R_1}\right) + \Psi_{3D}\left(\frac{z+z_1}{R_1}\right)\right] \cdot \end{aligned} \tag{22}$$

In Eq. (22), the first two terms correspond to the field in the 3D trap with no holes and the remaining terms correspond to the contribution of the hole.

6. Fields in 2D traps

We next turn to the 2D trap and present the approximate analytical equations for the field along an axis of the trap. The cross-sectional view of the RIT which is taken as an example for the discussion is shown in Fig. 7. In this trap the slit has been positioned on the top and bottom electrodes and consequently we will present the expression for the field along the y-axis. Unlike the detailed demonstrations we presented for the axially symmetric (3D) traps,

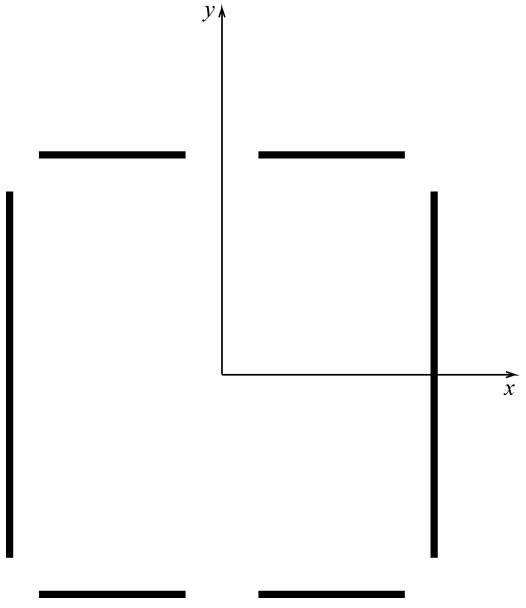

Fig. 7. Cross-section of the rectilinear ion trap.

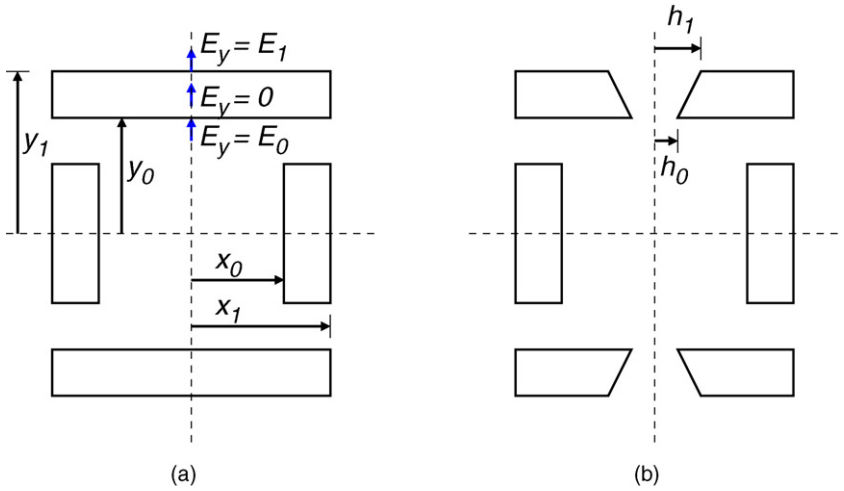

Fig. 8. (a) Schematic of an RIT with thick electrodes with no slits. (b) The same RIT in which the endcaps have slits.

here we will present just the expressions, leaving the verification of these equations to Section 7.

6.1. Contribution of the slit to the field

To get the analytical expression for the field in the 2D trap, the field has been derived in elliptic cylindrical co-ordinates and the contribution due to the slit on the electrode are expressed, as derived in Smythe [17], as

$$E_{\text{withslit}}(y) - E_{\text{noslit}}(y) = \frac{(E_1 - E_0)}{2}\left[-\text{sign}(y/h) + \frac{y/h}{\sqrt{(y/h)^2 + 1}}\right]. \tag{23}$$

$E_{\text{withslit}}(y)$ and $E_{\text{noslit}}(y)$ have the same connotation as $E_{\text{withhole}}(z)$ and $E_{\text{nohole}}(z)$ in the 3D case, h is the half-width of the slit, E_1 and E_0 are the y-components of the fields on either side of the electrode in the absence of the slit at the center of the electrode.

The field, $E_{2D}(y)$, inside the 2D traps can be expressed as

$$E_{2D}(y) = E_{\text{noslit}}(y) + \Delta E\left[\Psi_{2D}\left(\frac{y - y_0}{h}\right) + \Psi_{2D}\left(\frac{y + y_0}{h}\right)\right], \tag{24}$$

where

$$\Psi_{2D}(\eta) = \frac{1}{2}\left[-\text{sign}(\eta) + \frac{\eta}{\sqrt{\eta^2 + 1}}\right]. \tag{25}$$

Similar to 3D, here we treat the electrodes of the practical trap as two plates with slits, at a distance y_0 and y_1 along the y-axis, on the elctrodes from the trap centre.

Fig. 8 (a) presents the geometry of the RIT with electrodes having finite thickness and with no slits in the opposite electrodes. Also shown are the field orientations near those electrodes. Fig. 8(b) is the schematic of the same RIT with beveled slits on the endcap electrodes. The two different slit widths on the electrodes have dimensions h_0 and h_1.

Thus the contribution of the slits that would replace the E_{withslit} component in the 2D field Eq. (29) is

$$\begin{aligned} E_{\text{slit}}(y) = \; & E_1\left[\Psi_{2D}\left(\frac{y - y_1}{h_1}\right) + \Psi_{2D}\left(\frac{y + y_1}{h_1}\right)\right] \\ & -E_0\left[\Psi_{2D}\left(\frac{y - y_0}{h_0}\right) + \Psi_{3D}\left(\frac{y + y_0}{h_0}\right)\right]. \end{aligned} \tag{26}$$

For this expression to be used for mass analysers with same geometry parameters but with different slit width, the same constants evaluated for the original mass analyser are used and only the width of the slit h, on the endcap electrode is modified. The constants include ΔE and the multipole coefficients β_{2k}, $\beta'_{2(M+1)}$ and are to be evaluated numerically. None of these constants depend on h and their evaluation is done for a trap without any slit on the endcap electrodes.

6.2. $E_{noslit}(y)$

Analogous to the 3D geometries (Section 5.2) here again we need to evaluate the field without a hole in the electrodes. Using the same methodology we obtain

$$E_{\text{noslit}}(y) = \sum_{k=1}^{M} \beta_{2k} y^{2k-1} + \beta'_{2(M+1)} y^{2M+1}, \tag{27}$$

where β_{2k} refers to the even order multipoles. As in the 3D case the expression for field (Eq. (27)) contains an additional higher order term $\beta'_{2(M+1)}$ to match the numerically estimated field. $\beta'_{2(M+1)}$ is numerically estimated using the field at $y = y_0$ by the expression

$$\beta'_{2(M+1)} = \left(E_0 - \sum_{k=1}^{M} \beta_{2k} y_0^{2k-1}\right) / y_0^{2M+1}. \tag{28}$$

6.3. Electric field in the 2D trap

Again, similar to the 3D geometries, we have the composite expression for the field given by

$$\begin{aligned} E_{2D}(y) = \; & \sum_{k=1}^{M} \beta_{2k} y^{2k-1} + \beta'_{2(M+1)} y^{2M+1} \\ & + E_1\left[\Psi_{2D}\left(\frac{y - y_1}{h_1}\right) + \Psi_{2D}\left(\frac{y + y_1}{h_1}\right)\right] \\ & - E_0\left[\Psi_{2D}\left(\frac{y - y_0}{h_0}\right) + \Psi_{2D}\left(\frac{y + y_0}{h_0}\right)\right]. \end{aligned} \tag{29}$$

In Eq. (29), the first two terms correspond to the field in the 2D trap with no slits and the remaining terms correspond to the contribution of the slits in the electrodes.

Table 2
Values of constants in Eq. (22) for the Paul trap (z is in mm).

E_0	E_1	α_2	α_4	α_6	α'_8
141.59	−20.333	20.031	-1.1903×10^{-5}	-3.2079×10^{-6}	1.109×10^{-8}

7. Results and discussions

We next turn to verifying the validity of Eqs. (22) and (29) to describe the field within the 3D and 2D ion trap geometries, respectively. For doing this, we have chosen the Paul trap, the CIT and an arbitrary geometry, labelled as stepped ring electrode ion trap (SRIT), to verify the 3D electric field equation and the linear ion trap (LIT) and the RIT to verify the 2D electric field equation. In each case we have plotted, with circles, the electric field for an aperture dimension of 10% of the dimension of the trap and with crosses, the aperture dimension of 50% of the trap dimension.

To use Eqs. (22) and (29), two sets of constants are required to be evaluated numerically first. For a trap with no apertures, the electric field difference on either side of the electrode ΔE (obtained by evaluating E_0 and E_1), α_{2k}, $\alpha'_{2(M+1)}$ for the 3D trap needs to be evaluated and ΔE, β_{2k}, $\beta'_{2(M+1)}$ for the 2D trap needs to be evaluated. When these constants are inserted into the respective equations (Eq. (22) for 3D geometries and Eq. (29) for 2D geometries), they can be used to obtain the field along the principal axis for the traps with apertures of any size.

We begin with the verification of the 3D field equation first and then present the results for the 2D field equation.

7.1. Axially symmetric (3D) traps

7.1.1. The Paul trap

Fig. 9 (a) presents the schematic diagram of the Paul trap on which our simulations have been carried out. The table below the figure gives the dimensions of the geometric parameters in mm. In our simulations the ring electrode was kept at unit positive potential and the endcap electrodes were kept at ground potential. Table 2 presents the constants obtained for this trap geometry with no holes, these constants having been evaluated using the BEM [19].

Inserting the constants tabulated in Table 2 into Eq. (22) yielded the plot shown in Fig. 9(b) for $R_0/r_0 = 0.1$ (circles) and for $R_0/r_0 = 0.5$ (crosses). The field strength (in V/m) has been plotted along the ordinate while the distance from the centre of the trap plotted along the abscissa (in mm). The numerically generated fields for

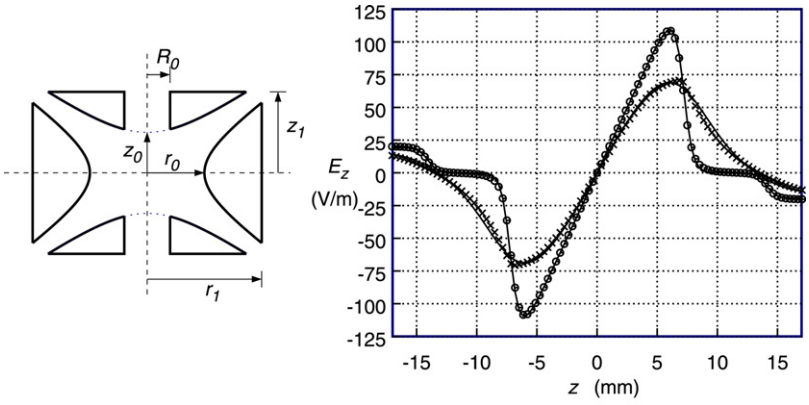

r_0	r_1	z_0	z_1	R_0
10	20	7.071	14.142	1.0(circle), 5.0(cross)

Fig. 9. (a) Cross-sectional view of Paul trap and (b) electric field plot along the axial direction. Circles correspond to $R_0/r_0 = 0.1$ and crosses to $R_0/r_0 = 0.5$. All dimensions of geometry parameters indicated in the table are in mm.

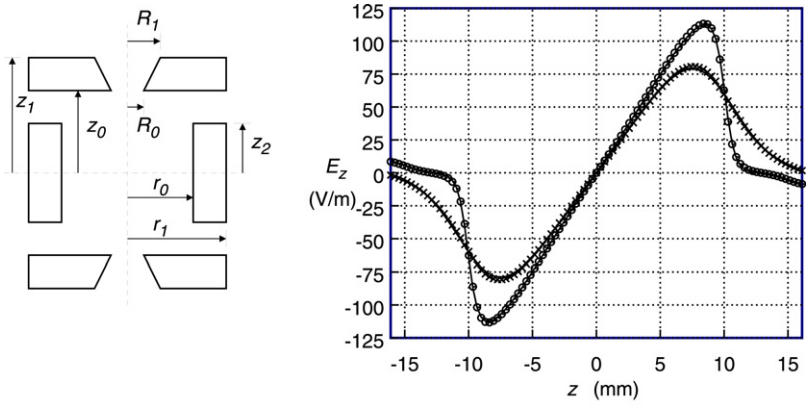

r_0	r_1	z_0	z_1	z_2	R_0	R_1
10	12	10	15	8	1.0(circle), 5.0(cross)	$2R_0$

Fig. 10. (a) Cross-sectional view of CIT and (b) electric field plot along z-axis. All dimensions of the geometry parameters given in the table are in mm.

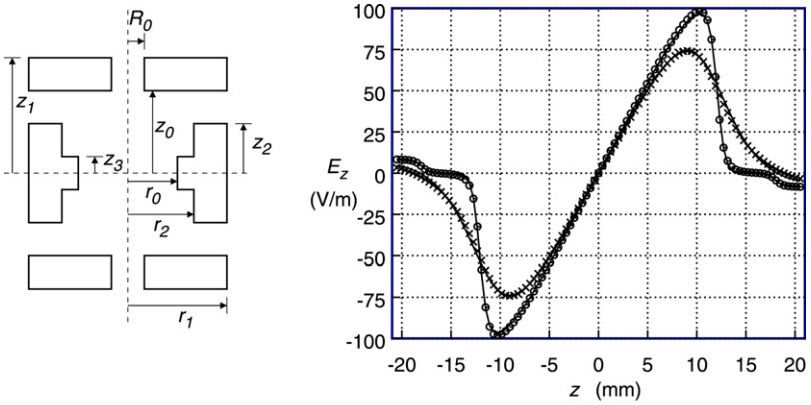

(a) (b)

r_0	r_1	r_2	z_0	z_1	z_2	z_3	R_0
10	15	12	12	18	9	2	1.0(circle), 5.0(cross)

Fig. 11. (a) Cross-section of SRIT and (b) electric field distribution along its z-axis. All dimensions of the geometry parameters given in the table are in mm.

these two different hole radii have also been included in the figure by continuous lines.

While the match between the field predicted by Eq. (22) and the field obtained numerically for $R_0/r_0 = 0.1$ is excellent, there is a marginal difference corresponding to the $R_0/r_0 = 0.5$ curve. This difference arises predominantly due to the variation in the dimension of z_0 which occurs when the aperture size is increased on hyperbolic electrodes. While this could, in principle, be corrected for by inserting the actual value of z_0, this has not been attempted here.

Another interesting feature of Eq. (22) may be observed in the curve corresponding to $R_0/r_0 = 0.1$. It should be noted that the length of the hole has been chosen to be large for the purpose of these simulations (the length is equal to the radius of the trap). Although this an exaggerated length, the field predicted by Eq. (22) closely follows the numerically obtained field, even flattening out within the aperture.

7.1.2. The CIT

Fig. 10 (a) presents the schematic diagram of the CIT geometry used in our simulations. The geometry parameters are given in the table associated with the figure and all the dimensions are in mm. For these simulations, the ring electrode was kept at unit positive potential and the endcap electrodes at ground potential.

The different constants obtained for the geometry are given in Table 3. Using these constants in Eq. (22) we have plotted the fields as shown in Fig. 10(b). The ordinate shows the field strength (in V/m) and the abscissa shows the distance (in mm) from the centre of the trap. The analytical field has been plotted as circles for $R_0/r_0 = 0.1$ and with crosses for $R_0/r_0 = 0.5$. Also superimposed on these plots, are the numerically computed fields which are shown for the corresponding hole dimensions. It should be noted here that the holes are bevelled and have two different radii.

It has been observed from the plot that the field distribution becomes smoother with the increase in hole radius. The thickness of the endcap electrodes (5 mm) considered are quite large compared with the trap dimension (10 mm). In spite of this the match between the field predicted by Eq. (22) and that obtained numerically for the two different hole sizes is excellent.

Table 3
Values of constants in Eq. (22) for CIT (z is in mm).

E_0	E_1	α_2	α_4	α_6	α'_8
122.676	−10.892	14.4516	4.081×10^{-2}	-7.732×10^{-4}	1.46736×10^{-6}

Table 4
Values of constants in Eq. 22 for SRIT (z is in mm).

E_0	E_1	α_2	α_4	α_6	α'_8
103.3785	−8.4085	10.997	3.074×10^{-3}	-1.213×10^{-4}	-1.0387×10^{-7}

7.1.3. The SRIT

Fig. 11 (a) presents the schematic diagram of an arbitrary trap, which is a variant of CIT and referred to as SRIT by [19]. The geometry parameters are given in the table associated with the schematic diagram. Here too the dimensions are in mm. This simulation was carried out with the ring electrode at unit positive potential and endcap electrodes at ground potential.

The various constants obtained numerically (using BEM [19]) for this geometry are tabulated in Table 4. Using these constants in Eq. (22) we obtained the plot shown in Fig. 11(b). The field strength in V/m, has been plotted along the ordinate and the distance from the center along the axial direction of the trap expressed in mm, has been plotted along the abscissa. As in earlier discussions, circles have been used for the field along the axis when $R_0/r_0 = 0.1$, and crosses have been used to for $R/r_0 = 0.5$.

Similar to the other axially symmetric (3D) geometries considered, the analytical approximation shows excellent matching even when the length of the hole is large.

7.2. Two dimensional traps

To verify the Eq. (29) to predict the field along the principal axis in 2D traps, we have considered the LIT and the RIT.

7.2.1. The LIT

Fig. 12 (a) presents the schematic diagram of the LIT geometry used in our simulations. The geometry parameters are given in the table below the figure. In our simulations, one pair of electrodes (along the x-axis) was kept at unit positive potential, and the other pair of electrodes was kept at ground potential.

The constants obtained for this geometry (using the BEM [7]) are given in Table 5. Inserting these constants in Eq. (29) we plot the

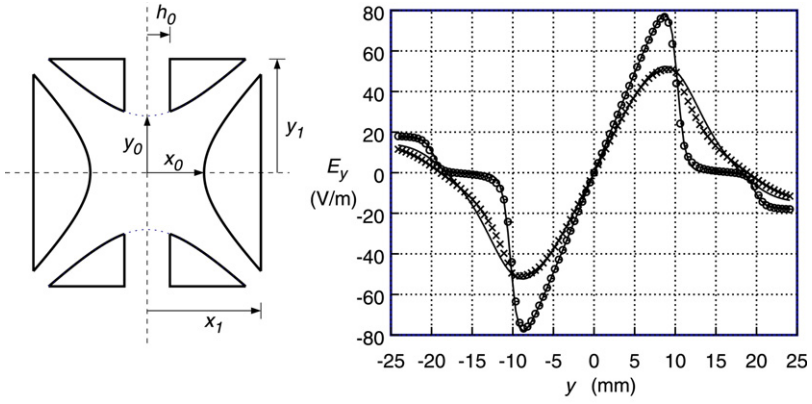

x_0	x_1	y_0	y_1	h_0
10	20	10	20	1.0(circle), 5.0(cross)

Fig. 12. (a) Cross-section of LIT and (b) electric field plot along y-axis for LIT. Circles have been used for $h_0/x_0 = 0.1$ and crosses for $h_0/x_0 = 0.5$. All dimensions of geometry parameters given in the table are in mm.

Table 5
Values of constants in Eq. 29 for LIT (y is in mm).

E_0	E_1	β_2	β_4	β_6	β'_8
100.13	−18.3848	10.01637	3.72694×10^{-5}	-6.971×10^{-7}	-3.7431×10^{-11}

Table 6
Values of constants in Eq. 29 for RIT (y is in mm).

E_0	E_1	β_2	β_4	β_6	β'_8
83.71563	−29.2785	10.964	1.6647×10^{-5}	-3.249×10^{-4}	6.546818×10^{-7}

field analytically in Fig. 12(b). The abscissa represents the distance from the centre of the trap towards the electrodes with apertures (in mm) and the ordinate shows the field strength (in V/m). The field has been obtained for $h_0/x_0 = 0.1$ (indicated by circles) and for $h_0/x_0 = 0.5$ (indicated by crosses). The numerically computed fields are superimposed on the analytically plotted curves for the corresponding slit dimensions. The smoothness of the curves increases with the increase in slit width.

In the LIT geometry considered, the thickness of the electrodes are large (10 mm). Even for such large aperture lengths, the analytical field shows excellent fit to the numerically obtained fields.

7.2.2. The RIT

Fig. 13 (a) presents the schematic diagram of the RIT geometry used in our simulations. Its geometry parameters are specified in the table below the figure. For simulation the electrode pair with no slit have been kept at unit positive potential while the electrode pair with slits have been at ground potential.

The constant terms obtained for this geometry (using the BEM [7]) are given in Table 6. Inserting these constants in Eq. (29), we plot the fields as shown in Fig. 13(b). The fields have been obtained for $h_0/x_0 = 0.1$ and for $h_0/x_0 = 0.5$, the former plotted with circles and the latter with crosses. The abscissa shows the distance in mm along y-axis of the trap and the ordinate indicates the field strength in V/m. The superimposed plots, shown as continuous lines, are the numerically computed fields for the corresponding slit dimensions. Here too the smoothness of the curves is improved as the slit width increases.

In the RIT geometry considered, the thickness of the electrodes are 5 mm which is large compared to the trap dimension. Even so, the analytically obtained field shows excellent match with the numerically obtained field.

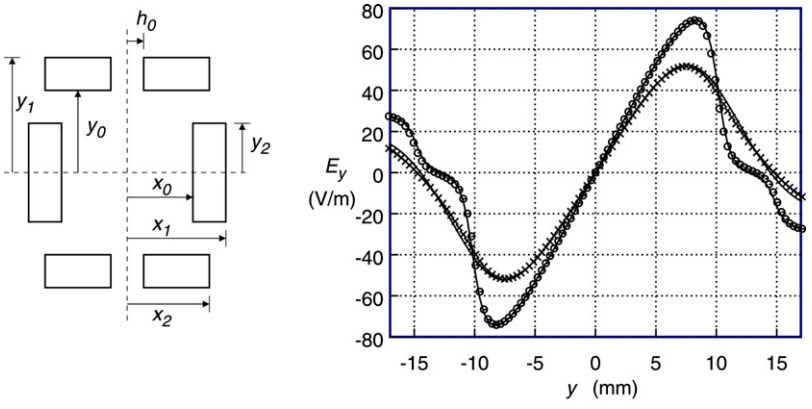

x_0	x_1	x_2	y_0	y_1	y_2	h_0
10	15	9	10	15	9	1.0(circle), 5.0(cross)

Fig. 13. (a) Cross-section of RIT and (b) electric field plot along y-axis for RIT. Circles represent the field for $h_0/x_0 = 0.1$ and crosses for $h_0/x_0 = 0.5$. All dimensions of geometry parameters indicated in the table are in mm.

8. Concluding remarks

This paper presented approximate analytical expression for the field along the principal axis in axially symmetric (3D) and 2D geometry ion traps. The expressions consisted of two parts. The first part is a modified truncated multipole expansion to approximate the field within the trap which has no apertures on their electrodes. The second part is an analytical expression corresponding to the contribution of the aperture on the two electrodes to the field in the vicinity of the electrodes. This latter expression incorporates the size of the aperture as well as thickness of the electrodes. Using these expressions (Eqs. (22) and (29)), it is now possible to estimate the field not just between the two electrodes with apertures but also to a distance just beyond the electrodes in axially symmetric (3D) and 2D geometry traps, respectively.

This work is of particular significance to miniaturized traps, especially at the MEMS scale (e.g., Blain et al. [4]) where ignoring the effect of fields close to the electrodes is not possible for two reasons. First, ion oscillations amplitudes are no longer small compared to trap dimensions and consequently the ion motion is indeed influenced by the field close to the electrodes. Second, in the fabrication of these devices, apertures on the one hand, and truncation of the electrodes on the other, will not scale in the same proportion as the trap dimensions. The proportionally "larger" apertures as well as truncation of the electrodes that these miniature traps have, will contribute more significantly to the inhomogeneity of the field within the trap than it happens in the case of the practical trap which are commercially available.

Immediate applications of this theory are in numerical trajectory simulations, whose region of validity will now extend up to and slightly beyond the apertures, unlike prior studies based purely on truncated multipole expansions. As a caution, we point out that the theory presented here relates only to the field on the principal axis of the trap. There may be a need in the future to explore the possibilty of generalizing this theory to the off-axis case as well.

References

[1] G.T. Abraham, A. Chatterjee, A.G. Menon, International Journal of Mass Spectrometry 231 (2004) 1.
[2] E. Beaty, Physical Review A 33 (1986) 3645.
[3] M.E. Bier, J.E.P. Syka, US Patent 5,420,425 (1995).
[4] M.G. Blain, S.R. Leah, D. Cruz, D.E. Austin, G. Wu, W.R. Plass, R.G. Cooks, International Journal of Mass Spectrometry 236 (2004) 91.
[5] J. Franzen, R.H. Gabling, M. Shubet, Y. Wang, in: R.E. March, J.F.J. Todd (Eds.), Practical Aspects of Ion Trap Mass Spectrometry, vol. 1, CRC Press, New York, 1995, p. 69.
[6] J.D. Jackson, Classical Electrodynamics, Wiley, New York, 1975.
[7] A. Krishnaveni, N.K. Verma, A. Menon, A.K. Mohanty, International Journal of Mass Spectrometry 275 (2008) 11.
[8] D.B. Langmuir, R. Langmuir, H. Shelton, R.F. Wuerker, US Patent 3,065,640 (1962).
[9] A.A. Makarov, Analytical Chemistry 68 (1996) 4257.
[10] R.E. March, R.J. Hughes, Quadrupole Storage Mass Spectrometry, Wiley–Interscience, New York, 1989.
[11] N.W. McLachlan, Theory and Applications of Mathieu Functions, Clarendon, Oxford, 1947.
[12] Z. Ouyang, G. Wu, Y. Song, H. Li, W.R. Plass, R.G. Cooks, Analytical Chemistry 76 (2004) 4595.
[13] W. Paul, H. Steinwedel, US Patent No. 2939952 (1960).
[14] W.R. Plass, R. Hongyan Li, R. Cooks, International Journal of Mass Spectrometry 228 (2003) 237.
[15] N. Rajanbabu, A. Chatterjee, A.G. Menon, International Journal of Mass Spectrometry 261 (2007) 159.
[16] N. Rajanbabu, A. Marathe, A. Chatterjee, A.G. Menon, International Journal of Mass Spectrometry 261 (2007) 170.
[17] W.R. Smythe, Static and Dynamic Electricity, McGraw-Hill, New York, 1950.
[18] M. Sudakov, International Journal of Mass Spectrometry 206 (2001) 27.
[19] P.K. Tallapragada, A.K. Mohanty, A. Chatterjee, A.G. Menon, International Journal of Mass Spectrometry 264 (2007) 38.
[20] E. Weber, Electromagnetic Fields: Theory and Applications. Vol. 1—Mapping of Fields, John Wiley & Sons, New York, 1950.
[21] G. Wu, R.G. Cooks, Z. Ouyang, International Journal of Mass Spectrometry 241 (2005) 119.